Electronic Supplementary Material (ESI) for Nanoscale.
This journal is © The Royal Society of Chemistry 2024

Supporting Information

Electrically Tunable Interlayer Recombination and Tunneling Behavior in WSe_2/MoS_2 Heterostructure for Broadband Photodetector

Chao Tan,[§a] Zhihao Yang,[§a] Haijuan Wu,[a] Yong Yang,[b] Lei Yang[a] and Zegao Wang[*a]

As shown in Figure S1, the top-gate voltage (x-axis) and bias voltage (y-axis) divide the conductivity of the device into four parts, which has the potential of multi-dimensional tunability [1, 2]. As shown in (e), zone A, B belong the state IV (the division of the state is shown in Figure 3), where both forward and reverse bias voltages drive a diffusion of electron carriers between WSe_2 and MoS_2 to generate the drain current. Zone C, D belongs the state II, where the heterostructure is a typical p-n junction. Hence, at zone C the forward bias leads to a diffusion current contributed to the diffusion of majority carriers, while the reverse bias generates a drift current attributed to the minority carriers at zone D [3, 4]. Moreover, it was observed that the depletion zone (state III) gets wider significantly with higher positive back-gate voltage. Wherein, the state IV remains unmoved, and the state II shifts towards left. However, with higher negative back-gate voltage, the depletion zone slightly widens, where the state IV and II shift to right.

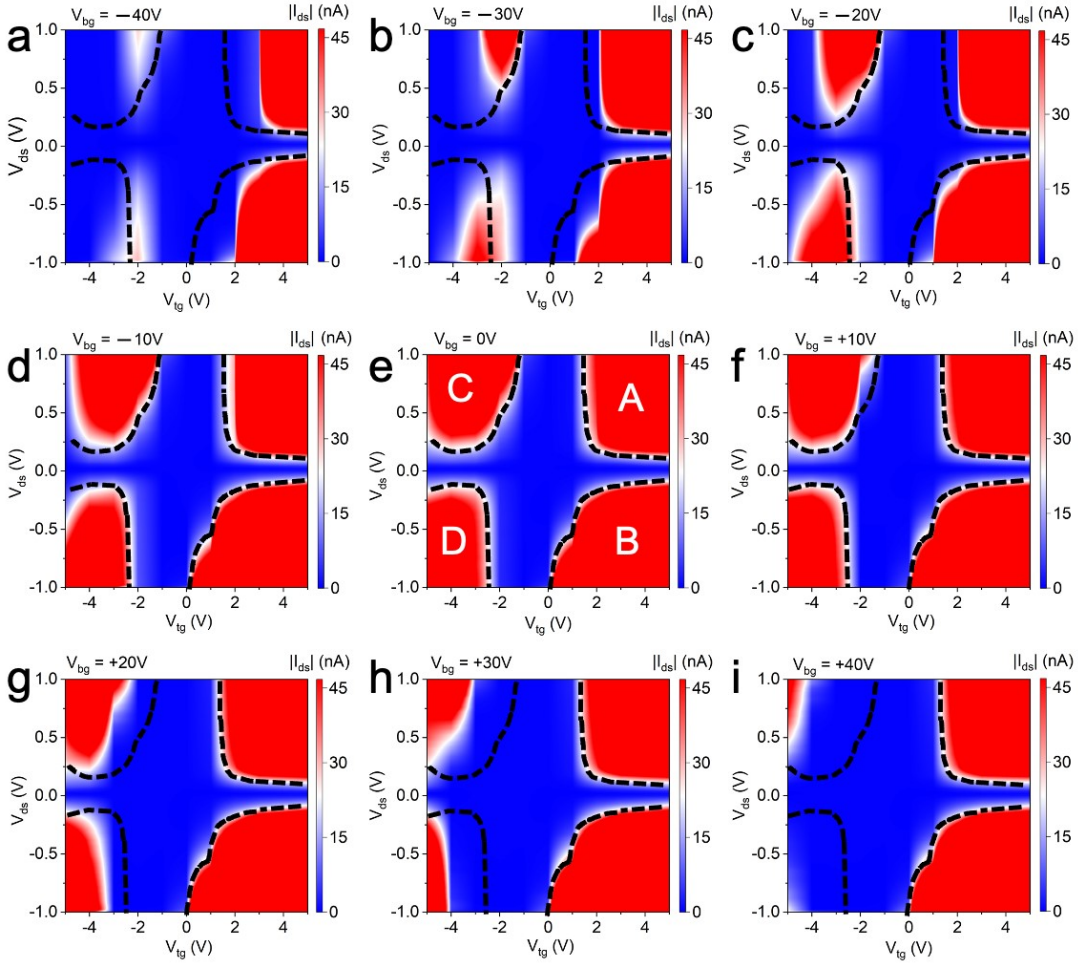

Figure S1 Transfer characteristics at varying bias voltages under different back-gate voltages. All the black dash lines are copied from that of (e), which presents the change of the transfer's contour color under different back-gate voltages.

At the p-i state (see Figure 3), the Fermi level starts to shift toward the conduction band in MoS_2 and the accumulated holes in WSe_2 diffuses into MoS_2, resulting in a diffusion current. With more positive V_{tg}, the carrier concentrations in WSe_2 and MoS_2 reach an equilibrium state. In the process, the variation of V_{tg} impedes the diffusion of majority carriers between WSe_2 and MoS_2. With further more positive V_{tg}, MoS_2 turns into the electron accumulation state and the electron concentration in MoS_2 becomes higher than that of WSe_2. Thus, the increase of V_{tg} benefits the diffusion current in the device until the state of i-n.

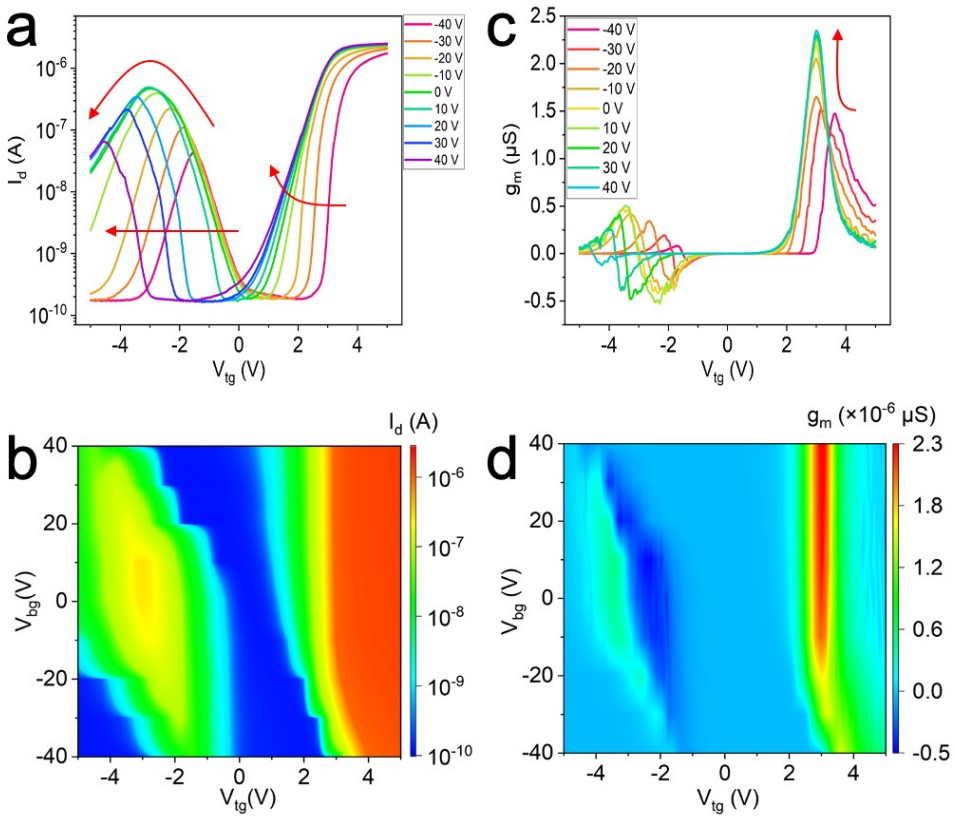

Figure S2 (a, b) Transfer and (c, d) transconductance characteristics under different back-gate voltages at fixed bias voltage of 1 V.

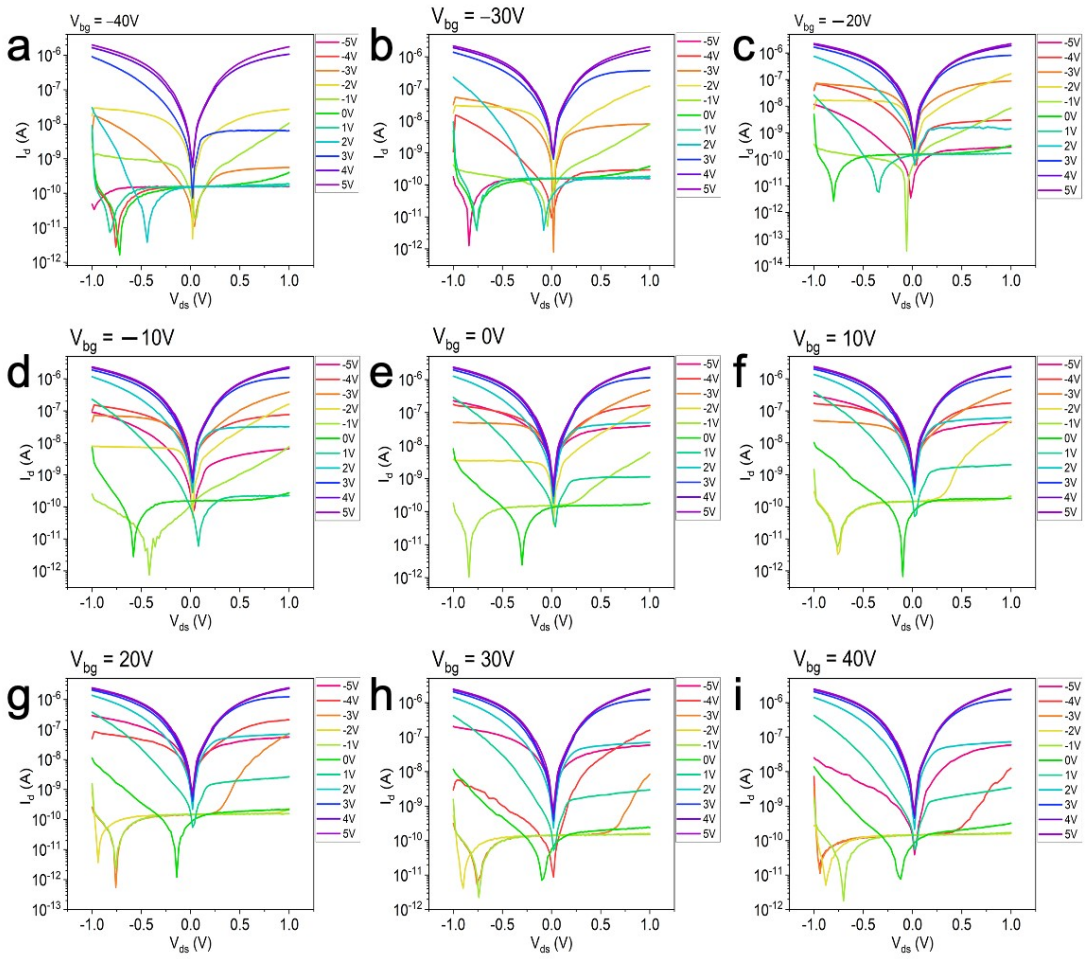

Figure S3 Output curves under different top- and back-gate voltages.

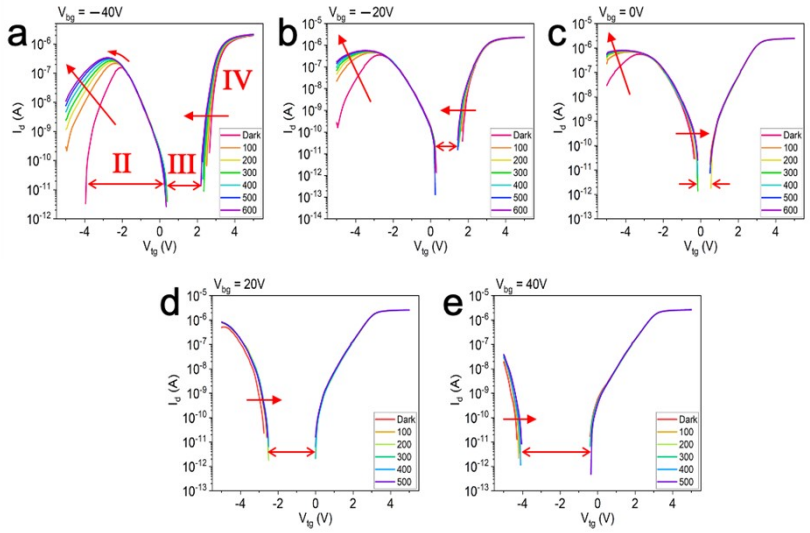

Figure S4 Transfer curves under illumination of 400 nm wavelength with different light intensity at different back-gate voltages and fixed bias voltage of 1 V. The marked

regions (II, III and IV) in the figures represent different electrical states of the device at different top-gate voltages. It shows that the state II widens and the state IV shifts to left with increasing light intensity.

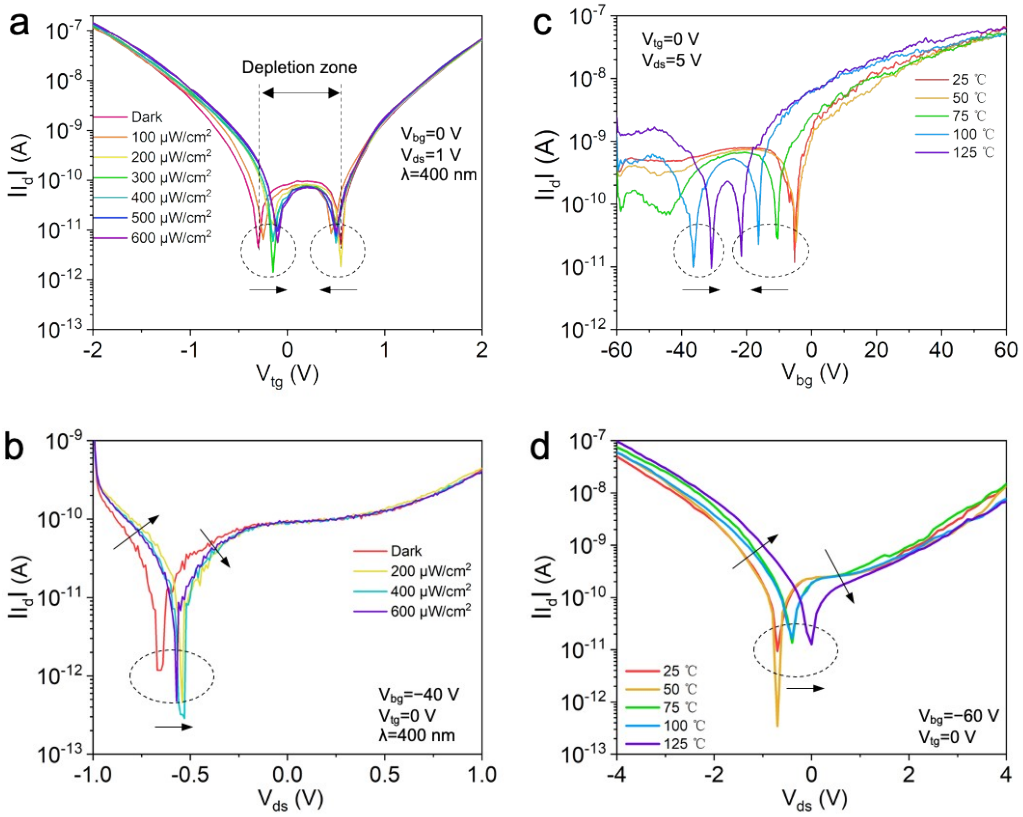

Figure S5 (a) Transfer characteristics under illumination of 400 nm wavelength with different light intensity at fixed back-gate voltage of 0 V and fixed bias voltage of 1 V. (b) Output characteristics under illumination of 400 nm wavelength with different light intensity at fixed top- and back-gate voltages of 0 V and –40 V, respectively. (c) Transfer characteristics under different temperatures at fixed top-gate voltage of 0 V and fixed bias voltage of 5 V. (d) Output characteristics under different temperatures at fixed top- and back-gate voltages of 0 V and –60 V, respectively.

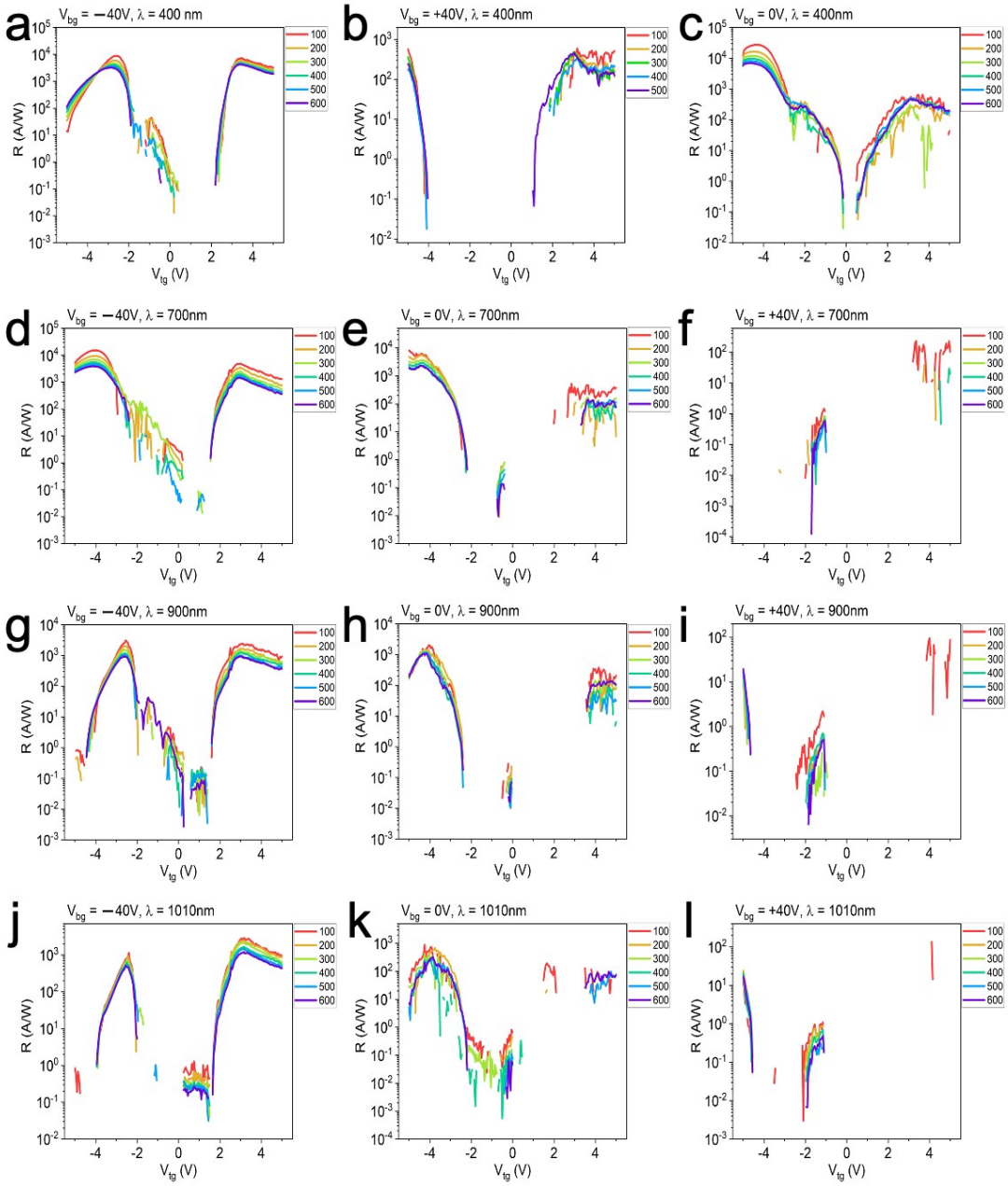

Figure S6 The responsivity curves under illumination of 400, 700, 900 and 1010 nm wavelengths with different light intensity at different top- and back-gate voltages and fixed bias voltage of 1 V.

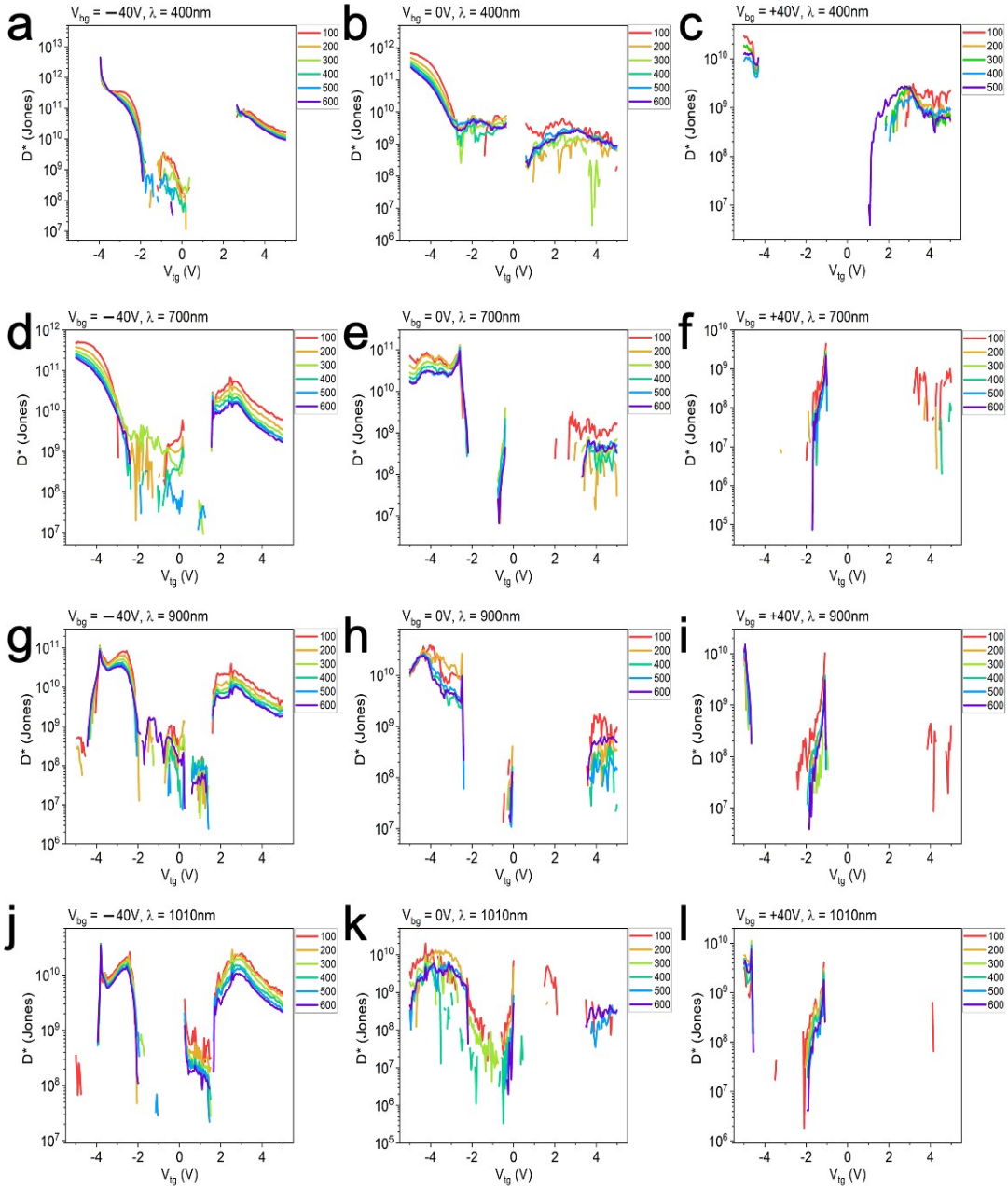

Figure S7 The specific detectivity curves under illumination of 400, 700, 900 and 1010 nm wavelengths with different light intensity at different top- and back-gate voltages and fixed bias voltage of 1 V.

Table S1 Performance comparison of 2D heterostructure-based photodetectors.

Materials Configuration	**Wavelength nm**	**Responsivity A/W**	**Specific Detectivity Jones**	**Ref.**
WSe_2/CuO	530	0.28×10^{-3}	0.19×10^{10}	[5]
WSe_2/MoS_2	532	1.392	7.78×10^{12}	[6]
b-AsP/WSe_2	275	244	2.27×10^{12}	[7]

WSe_2/hBN	532	170	1.1×10^{12}	[8]
WSe_2/MoS_2	532	2700	5×10^{11}	[9]
MoS_2/WSe_2	633	8	2.93×10^{11}	[10]
WS_2/WSe_2/p-Si	405	3.72	2.39×10^{12}	[11]
Ta_2NiSe_5/WSe_2	638	0.04×10^{-3}	3.6×10^{5}	[12]
InSe/WSe_2	633	5300	10^{11}	[13]
PtS_2/WSe_2	635	0.42	1.37×10^{12}	[14]
WSe_2/MoS_2	400	27445	10^{13}	**This work**
WSe_2/MoS_2	1010	2827	10^{10}	**This work**

Reference

[1] X. Ji, Z. Bai, *et al. ACS Omega* **2022**, 7(12):10049-10055.
[2] M. Yang, Y. Lu, *et al. Applied Physics Letters* **2022**, 121(4):043501.
[3] G.H. Shin, C. Park, *et al. Nano Lett* **2020**, 20(8):5741-5748.
[4] H.B. Jeon, G.H. Shin, *et al. Advanced Electronic Materials* **2020**, 6(7):2000091.
[5] R.P. Patel, P.M. Pataniya, *et al. Sensors and Actuators A: Physical* **2023**, 356:114339.
[6] R. Mao, Z. Liu, *et al. Applied Physics Express* **2023**, 16(3):034001.
[7] F. Zhao, D. Wang, *et al. Applied Physics Letters* **2023**, 122(15):151105.
[8] S. Ghosh, A. Varghese, *et al. Nature Communications* **2021**, 12(1):3336.
[9] G.H. Shin, C. Park, *et al. Nano Letters* **2020**, 20(8):5741-5748.
[10] Y. Xiao, J. Qu, *et al. Frontiers of Optoelectronics* **2022**, 15(1):41.
[11] Z. Huang, M. Yang, *et al. Science China Materials* **2023**, 66(6):2354-2363.
[12] P. Xiao, S. Zhang, *et al. Sensors* **2023**, 23(9):4385.
[13] C.R. Paul Inbaraj, R.J. Mathew, *et al. ACS Applied Materials & Interfaces* **2023**, 15(15):19121-19128.
[14] C. Tan, S. Yin, *et al. ACS Nano* **2021**, 15(5):8328-8337.